A discontinuous Galerkin method for solving the shallow water equations

Daniela Vignali
daniela.vignali@tecnico.ulisboa.pt

Instituto Superior Técnico, Universidade de Lisboa, Portugal

May 2023

Abstract

Recently, energy requirements have proliferated in many countries all around the globe. Tidal energy is one of the most promising energy sources, due to its predictability, low environmental impact and no occupation of land. However, high investment costs and restricted sites are available, which slow development and improvement. Understanding the tidal energy resources in the framework of new tidal stream technologies is essential to have a clear view of the power generation available. The shallow water equations have been successfully applied in describing tidal waves and tidal analysis. The shallow water system is a set of partial hyperbolic differential equations. This thesis focuses on developing a numerical model with the Discontinuous Galerkin Method to solve these types of equations.
The Discontinuous Galerkin method allows the conservation of mass and momentum on an element basis, and is well suited for unconstructed meshes The conservation of variables guarantees a correct calculation of the flow rate, the momentum flux in the local field and the water depth. The model has been developed in one-dimensional and two-dimensional versions. The first model has been simulated with a bump. The analysis of the error guarantees the accuracy of the solution. The second model has been simulated in a uniform solution, which presents good results with some concerns.

Keywords: tidal energy, shallow water equations, Discontinuous Galerkin method, momentum flux, local field

1. Introduction

Tides occur as a result of a non-uniform gravitational field. They respond under the gravitational forces of the Moon, Sun and other astronomical bodies. On top of this, tides are affected by the presence of continents, variable water depth and seabed shape, which create a more complicated scheme and determine a significant variation in the tidal range around the world. The amplitude can move from less than 1 m in the deep ocean up to 11.7 m in the coastal region as the Bay of Fundy (Canada), or Bristol Channel (UK). [5] Two main mechanisms define the increase in tidal amplitude closer to shore: first, the narrowing of a channel or an estuary, which leads to a concentration of energy in the tide, and second, the magnified intersection between incoming and reflected components of the tide.[3] This natural resonance, with the standing wave shape, is obtained when the width of the continent's coastline is around one-fourth of the tidal mode wavelength. [5]
Currently, there are three main options for producing energy from coastal tides: the barrage requires the construction of a dam across a bay or an estuary, to exploit the potential energy between the rise and fall of the tides; the tidal turbine involves the deployment of devices to extract energy from tidal streams; the tidal fence is a hybrid between the barrage and the tidal turbine.

1.1. Numerical methods

The discontinuous Galerkin method is a combination of the finite element and the finite volume. The Discontinuous Galerkin has features from both numerical methods, such as: the capability to model flows with significant horizontal velocity, direct implementation of boundary conditions through a numerical flux, suitability with unstructured grids to simulate complex geometries and offer higher accuracy within the flow field.
The method allows easy implementation of the TVD Runge-Kutta time integration scheme as each element is solved individually and one element is connected to the surrounding elements by boundary fluxes. The discontinuity can be easily resolved in this case because the nodes connecting the elements have two values [4]. This method is strongly suitable for high-order formulation and scheme presenting discontinuity. On the other hand, it is high storage and high computational requirements.

2. Tidal turbine classification

The European Marine Energy Centre classifies tidal stream turbines into four categories: axial-flow turbines, cross-flow axis turbines, oscillating devices and Venturi effect. They are described below, however other options are being studied [1, 2]:

- Horizontal axis turbines: they follow the same concept as wind turbines, which extract energy from moving air, while tidal horizontal axis turbines are crossed by water to produce energy.

- Cross-flow axis turbine: as previously mentioned their extraction of energy is similar to windmills, but their axis is perpendicular to the flow direction, and it can be mounted vertically or horizontally.

- Oscillating hydrofoil: these devices are attached to an arm and move up and down, where the hydrofoil sections are thrust sidewards by the flow instead of having rotational components.

- Enclosed tips (Venturi effect): they are equipped with a funnel-shaped shell, which concentrates the flow passing through the turbine, and the structure is completely submerged in the current. It can be installed vertically or horizontally.

EMEC recently added two new categories:

- Archimedes screw: it is a spiral-shaped device, the turbine unsheathes the tidal stream power while the water flows up and through the helix rotating the turbine. Two centuries ago, it had been suggested as a reverse machine, alias a turbine. Even so, it has been studied as an option in the tidal stream field only in the last 20 years, without an actual complete project deployed.

- Tidal kite: it is tied up to the seabed by a tether and equipped with a turbine below the wings. It draws an eight-shape trajectory to increase the water velocity passing through the turbine. Indeed it is developed to low-speed current and the kite structure pushes the turbine to feel a speed faster than the actual flow rate.

3. Swallow water model

The shallow water equations have been used to describe the approximate progression of long waves in small water depths. This model can be derived from a control volume analysis of a fluid element with an infinitesimal two-dimensional area and the entire water depth. To follow this analysis, some assumptions are necessary:

1. The flow is incompressible.
2. The free surface perturbation ζ is orders of magnitude smaller than the wavelength.
3. The diffusion of the momentum is negligible, which means the horizontal component of the hydrostatic gradient defines the flow direction.

The control volume is a cylinder with Γ as vertical walls, the seabed as the bottom boundary and the free surface as the upper boundary. The free surface perturbation at the boundary Γ is $\zeta(\theta, t)$, where θ is the linear coordinate of the boundary. The seabed bathymetry is represented by b(x,y).

The volume control analysis can be simplified to a two-dimensional system, where the velocity depends on time and horizontal coordinates. The domain is Ω and the boundary is Γ with $\mathbf{n}$ the outgoing normal. The conditions at the boundary are: the seabed is impermeable

$$(\mathbf{v} \cdot \mathbf{n})_b = 0 \tag{1}$$

and the free surface varies with the fluid

$$(\mathbf{v} \cdot \mathbf{n})_\zeta = 0 \tag{2}$$

The mass conservation equation on the control volume is given by

$$\frac{d}{dt} \int_A \int_b^\zeta \rho dz dA + \int_\Gamma \int_b^\zeta \rho \left(\mathbf{v} \cdot \mathbf{n}\right) dz d\Gamma = 0 \tag{3}$$

Moving to the two-dimensional system by integrating into z, since the velocity is vertically uniform. Furthermore, the equation can be divided by the density of the fluid and applied the Gauss theorem, to obtain

$$\begin{aligned} \frac{d}{dt} \int_A h dA + \int_\Gamma \int_b^\zeta h \mathbf{v} \cdot \mathbf{n} d\Gamma = \\ \int_A \left(\frac{\partial h}{\partial t} + \nabla \cdot (h\mathbf{v}) \right) dA = 0 \end{aligned} \tag{4}$$

The momentum balance on the fixed control volume follows a similar procedure of the conservation of mass. Given the fact the piezometric pressure and the velocity are uniform in the depth coordinate, the balance is respected in a three-dimensional space as in a two-dimensional space. The local pressure is defined as $p(z) = \rho g(\zeta - z)$, where $h = (\zeta - z)$. It is important to remember that $z = 0$ is the mean free surface level, and below it, z is negative, while the free surface perturbation ζ can assume positive or negative values.

The momentum balance for the control volume is

$$\frac{d}{dt} \int_V \rho \mathbf{v} dV + \int_S \rho \mathbf{v} \left(\mathbf{v} \cdot \mathbf{n}\right) dS = - \int_S p \mathbf{n} dS \tag{5}$$

The integral of the pressure can be reformulated, to obtain the momentum equation written as

$$\begin{aligned} \frac{d}{dt} \int_A \int_b^\zeta \rho \mathbf{v} dz dA + \int_\Gamma \int_b^\zeta \rho \mathbf{v} \left(\mathbf{v} \cdot \mathbf{n}\right) dz d\Gamma = \\ - \int_A \nabla \zeta \rho g h dA \end{aligned} \tag{6}$$

The flow is incompressible, as the assumption of the model, so the equation can be divided by the density ρ and integrated into z, and applying the Gauss theorem, the final equation is

$$\frac{d}{dt}\int_A h\mathbf{v}dA + \int_A \nabla\cdot(h\mathbf{v}\times\mathbf{v})\,dA = -\int_A \nabla\zeta ghdA \tag{7}$$

4. The Runge-Kutta Discontinuous Galerkin Method for one-dimensional shallow water equations

The shallow water equations can be presented in the conservative form as

$$\frac{\partial\mathbf{q}}{\partial t} + \frac{\partial\mathbf{F}}{\partial x} = \mathbf{s}, \tag{8}$$

with $x \in [0, L]$ and $t \in [0, \mathcal{T}]$. The $\mathbf{q}$ represents the vector of conservative variables, $\mathbf{F}$ is the flux vector and $\mathbf{s}$ describes the source term associated with the variation in the surface and the effect of fluid friction, are expressed by

$$\mathbf{q} = \begin{pmatrix} h \\ uh \end{pmatrix}, \quad \mathbf{F} = \begin{pmatrix} uh \\ hu^2 + \frac{1}{2}gh^2 \end{pmatrix}, \tag{9}$$

$$\mathbf{s} = \begin{pmatrix} 0 \\ -gh\dfrac{db}{dx}. \end{pmatrix}. \tag{10}$$

The sea-bed bathymetry $b(x)$ is a given data. The system of equations 8 requires initial conditions $\mathbf{u}(x, 0)$, and boundary conditions $\mathbf{u}(0, t)$ and $\mathbf{u}(L, t)$ to be introduced later.[6]

The computational domain I is divided into a set of N elements I_e non-overlapping one another, with length Δx_e and defined as

$$I_e = \left[x_e - \frac{1}{2}\Delta x_e\,,\, x_e + \frac{1}{2}\Delta x_e\right] \tag{11}$$

where x_e is the middle point of the element. There are two types of boundaries: internal edges Γ^{int}, when the edge of the element is inside of the space I and external edges Γ^{bc}, which define the boundary conditions of the domain and interact with the ghost element. The normals are pointing outward, from I_e to I_i is called $\hat{n}_{ei}$. Consequently, the opposite normal pointing from I_i toward I_e is called $\hat{n}_{ie}$ and it has the inverse value of $\hat{n}_{ei}$, $\hat{n}_{ei} = -\hat{n}_{ie}$ and they assume the following values

$$\begin{aligned} \hat{n}_{ei} &= +1, \\ \hat{n}_{ie} &= -1. \end{aligned} \tag{12}$$

The external boundaries are defined through two ghost elements Ω_b^{bc}.

4.1. Weak formulation

The definition of the solution $\mathbf{q}$ needs an approximation $\mathbf{q}_h$ for a given time instant $t \in [0, T]$, which is classified into a finite dimensional space $W_h = W_h^k \equiv \{w : w\,|I_e \in P^k(I_e), 1 \le e \le N\}$, where $P^k(I_e)$ is the space of the polynomials in I_e of degree up to k, which weakens the formulation through the following steps.

The system of equations (8) is multiplied by a set of arbitrary smooth functions, called test functions $\phi(x)$, and then integrated into I_e.

$$\int_{I_e}\frac{\partial\mathbf{q}}{\partial t}\,\phi\,dx + \int_{I_e}\nabla\cdot\mathbf{F}\,\phi\,dx = \int_{I_e}\mathbf{s}\,\phi\,dx. \tag{13}$$

Afterwards, the flux is integrated by parts, and considering the discontinuity of the method, the fluxes are substituted by the numerical fluxes $\mathbf{H}$, which depend on the two elements sharing the edge and the outward normal. [6]

$$\begin{aligned} \int_{I_e}\frac{\partial\mathbf{q}}{\partial t}\phi dx - \int_{I_e}\mathbf{F}\frac{d\phi}{dx}dx + \Big(\mathbf{F}(q_{ei})\hat{n}_{ei}\phi\Big) \\ + \Big(\mathbf{F}(q_{ej})\hat{n}_{ej}\phi\Big) = \int_{I_e}\mathbf{s}\,\phi dx. \end{aligned} \tag{14}$$

4.2. The Roe flux function

The assessment of the eigenvalues and eigenvector of the flux in the shallow water model can be solved by the Roe flux function, which requires the equation 8 in a quasi-linear form

$$\frac{\partial\mathbf{q}}{\partial t} + \mathbf{A}\frac{\partial\mathbf{q}}{\partial x} = \mathbf{s} \tag{15}$$

$$\mathbf{A} = \frac{\partial\mathbf{F}}{\partial q} = \begin{pmatrix} 0 & 1 \\ gh - v^2 & 2v \end{pmatrix} \tag{16}$$

Given the states $\mathbf{q}_{ei}$ and $mathbfq_{ie}$ the Roe's flux function is presented as

$$\begin{aligned} \mathbf{H}_{ei} = (q_{ei},\, q_{ie},\, \hat{n}_{ei}) = \\ \frac{1}{2}\left(\mathbf{F}_{ei}\mathbf{n_{ei}} + \mathbf{F}_{ie}\mathbf{n_{ie}} - |\mathbf{A}_m|((q_{ei} - q_{ie})\right) \end{aligned} \tag{17}$$

when the matrix $\mathbf{A}_m$ is a function of the mean value of conservative value

$$q_{ei_m} = q_{ie_m} = \frac{1}{2}(q_{ei} + q_{ie}) \tag{18}$$

The same equation can be obtained in the opposite direction. Concluding that

$$\mathbf{H}_{ei} = -\mathbf{H}_{ie} \tag{19}$$

4.3. Element transformation

The transformation to a master element is a convenient method for simplifying the computation. The master element is defined as $\hat{I} = [-1,\, 1]$ and ξ as local coordinate. The transformation is determined as

$$\xi = \frac{2}{\Delta x_e}(x - x_e) \tag{20}$$

where Δx_e and x_e are, respectively, the length and the middle point of the element I_e

4.4. Legendre polynomials and system of equation

The Legendre polynomial $p_m(\xi)$ is the option selected as a test function, thus the solution of k^{th}-order results in

$$q(\xi,t) \;=\; \sum_{m=0}^{k} p_m(\xi)\,\mathbf{q}_m(t) \tag{21}$$

where the m-order polynomial multiplies the conservative variables vector, presented as

$$\mathbf{q}_m \;=\; \begin{pmatrix} h_m \\ (hu)_m \end{pmatrix} \tag{22}$$

The Legendre polynomials are orthogonal over the defined interval $[-1\,,\,1]$, thus

$$\int_{-1}^{1} p_m(\xi)\,p_n(\xi)\,d\xi \;=\; \delta_{mn} \quad \delta_{mn} \;=\; \begin{cases} 1, & m \;=\; n \\ 0, & m \;\neq\; n \end{cases} \tag{23}$$

These polynomials are attainable using the subsequent recurrence equations

$$p_{n+1}(\xi) = \frac{\sqrt{n+\frac{3}{2}}}{n+1}\Big(\,(2n+1)\,p_n\;\xi - n\,p_{n-1}\Big) \tag{24}$$

with $1 < n < k$. Implementing the Legendre polynomial as smooth test function into 14, and applying the Legendre orthonormality property obtains

$$\begin{aligned} \frac{\Delta x}{2}\,\frac{\partial \mathbf{q}_n}{\partial t} \;-\; \int_{-1}^{1} \mathbf{F}\,\frac{dp_n}{d\xi}d\xi \;+\; \mathbf{H}_{ei}\,p_n(-1) \\ +\,\mathbf{H}_{ej}\,p_n(1) \;=\; \frac{\Delta x}{2}\int_{-1}^{1} \mathbf{s}\,p_n d\xi \end{aligned} \tag{25}$$

This system of formulae for each segment I_e can be revised as

$$\frac{\partial \mathbf{q}_n}{\partial t} \;=\; \tilde{\mathbf{F}}_n \;-\; \tilde{\mathbf{H}}_n \;+\; \tilde{\mathbf{S}}_n \;=\; \boldsymbol{\mathcal{R}}_n(q) \tag{26}$$

where $\boldsymbol{\mathcal{R}}_n$ is defined as the residual, it will be used in the chapter 4.6, and the other vectors are described by

$$\tilde{\mathbf{F}}_n \;=\; \frac{2}{\Delta x}\int_{-1}^{1} \mathbf{F}(\mathbf{q})\,\frac{dp_n}{d\xi}d\xi; \tag{27}$$

$$\tilde{\mathbf{H}}_n \;=\; \frac{2}{\Delta x}\left(\mathbf{H}_{ei}p_n(-1) \;+\; \mathbf{H}_{ej}p_n(1)\right); \tag{28}$$

$$\tilde{\mathbf{S}}_n \;=\; \int_{-1}^{1} \mathbf{s}\,\phi_n d\xi \tag{29}$$

4.5. Integrals discretization

The integration is computed on the master element throughout the Gauss-Legendre quadrature rule with r points (ξ_b) and weights w_b, the method applied on the flux gives

$$\tilde{\mathbf{F}}_n \;=\; \sum_{b=1}^{g} w_b \mathbf{F}(q(\xi_b))\,\frac{\partial p_n(\xi_b)}{\partial \xi} \tag{30}$$

For polynomials with degrees up to $2r-1$, the Gauss-Legendre quadrature is accurate.[6] The same procedure is practised on the source term,

$$\tilde{S}_n \;=\; \sum_{b=1}^{g} w_b S(\xi_b) p_n(\xi_b) \tag{31}$$

4.6. Time integration

$\boldsymbol{\mathcal{R}}_n(q)$ is required for the discretization of the progression in time of the system of equations 26, an explicit third-order total variation diminishing (TVD) Runge-Kutta method has been used as follows:

$$\begin{aligned} q_n^{(1)} \;&=\; q_n^{(0)} \;+\; \Delta t \boldsymbol{\mathcal{R}}_n(q^{(0)}) \\ q_n^{(2)} \;&=\; \frac{3}{4}q_n^{(0)} \;+\; \frac{1}{4}q_n^{(1)} \;+\; \frac{1}{4}\Delta t \boldsymbol{\mathcal{R}}_n(q^{(1)}) \\ q_n^{(3)} \;&=\; \frac{1}{3}q_n^{(0)} \;+\; \frac{2}{3}q_n^{(2)} \;+\; \frac{2}{3}\Delta t \boldsymbol{\mathcal{R}}_n(q^{(2)}) \end{aligned} \tag{32}$$

where superscript numbers are the progression in time and zero refers to the initial condition imposed.[6]

5. The Runge-Kutta Discontinuous Galerkin Method for two-dimensional shallow water equations

The equations can be presented in the conservative form

$$\frac{\partial \mathbf{q}}{\partial t} + \nabla \mathbf{F}(\mathbf{q}) = \mathbf{s}, \tag{33}$$

and each variable is a vector

$$\mathbf{q} = \begin{pmatrix} h \\ uh \\ vh \end{pmatrix}, \tag{34}$$

$$\mathbf{F} = \begin{pmatrix} uh & vh \\ hu^2 + \frac{1}{2}gh^2 & uvh \\ uvh & hv^2 + \frac{1}{2}gh^2 \end{pmatrix}, \tag{35}$$

$$\mathbf{s} = \begin{pmatrix} 0 \\ -gh\dfrac{db}{dx} \\ -gh\dfrac{db}{dy} \end{pmatrix}. \tag{36}$$

The sea-bed bathymetry $b(x)$ is a given data. The computational domain Ω is subdivided into a set of N elements Ω_e of a triangular shape and non-superimposed one another. The boundary conditions are introduced by designing ghost elements Ω_b^{bc} constituted by only one edge e_b^{bc}. The elements' boundaries are divided into two sets, internal edges Γ^{int} when the edge of the element is inside of the space Ω, and external edges Γ^{bc}, which define the boundary conditions of the domain and interact with the ghost elements. The nodes and edges go from 0 to 2 counterclockwise and the edge has the number of the opposite node. Therefore, each edge presents three indexes: in the superscript, the number relates to the position in the master element, in the subscript, first the belonging element after the neighbour or ghost element, as presented in figure 1.[6]

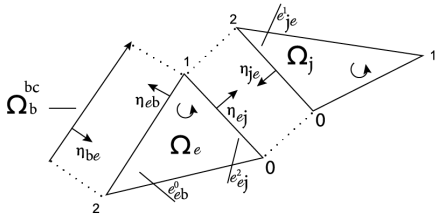

Figure 1: Representation of the tangents and the normals on the global space from element Ω_e and the connection with the boundary and the neighbour element Ω_j

5.1. Weak formulation

The system of equation is multiplied with a set of arbitrary smooth called test functions $\phi \in \Re^2$, followed by the integration over an element Ω_e.

$$\int_{\Omega_e} \frac{\partial q}{\partial t}\,\phi d\Omega + \int_{\Omega_e} \nabla \mathbf{F}\,\phi d\Omega = \int_{\Omega_e} \mathbf{s}\,\phi d\Omega \tag{37}$$

Afterwards, the flux is integrated by part and following the element boundaries previously described, the edges' flux has to be divided into internal and boundary condition. The fluxes are substituted by a numerical flux $\mathbf{H}$,[6] and result in

$$\begin{aligned}&\int_{\Omega_e} \frac{\partial \mathbf{q}}{\partial t}\,\phi d\Omega + \int_{\Omega_e} \mathbf{F}(\mathbf{q})\cdot\nabla\phi d\Omega \\ &+ \sum_{\Gamma_e^{int}} \int_{e_{ei}} \mathbf{H}(\mathbf{q}_{ei};\mathbf{q}_{ie};\mathbf{n}_{ei})\phi d\Gamma \\ &+ \sum_{\Gamma_e^{bc}} \int_{e_{eb}} \mathbf{H}(\mathbf{q}_{eb};\mathbf{q}_b^{bc};\mathbf{n}_{eb})\phi d\Gamma = \int_{\Omega_e} \mathbf{s}\,\phi d\Omega\end{aligned} \tag{38}$$

The numerical flux functions have the same structure as the one-dimensional case, therefore the Lax-Friedrichs flux is given by

$$\begin{aligned}\mathbf{H}(\mathbf{q}_{ei},\,\mathbf{q}_{ie},\,\mathbf{n}_{ei}) = \frac{1}{2}\mathbf{F}(\mathbf{q}_{ei})\,\cdot\,\mathbf{n}_{ei} + \frac{1}{2}\mathbf{F}(\mathbf{q}_{ie})\,\cdot\,\mathbf{n}_{ie} \\ - \frac{1}{2}\lambda_{\max}(\mathbf{q}_{ie} - \mathbf{q}_{ei})\end{aligned} \tag{39}$$

The maximum eigenvalue is computed using

$$\lambda_{\max} = \max\left(\lambda_{\max}(\mathbf{q}_{ei}),\,\lambda_{\max}(\mathbf{q}_{ie})\right) \tag{40}$$

with $\lambda_{\max} = |\mathbf{v}\cdot\mathbf{n}| + c$, see [6] for details.

5.2. Element transformation

The transformation T_e is the map of $\hat{\Omega}$ on Ω_e.

$$T_e : \begin{cases} x = x(\xi,\eta) \\ y = y(\xi,\eta) \end{cases} \tag{41}$$

Let consider that the functions derivation of x and y respect to ξ and η are continuous, then the infinitesimal transformation $d\xi\ d\eta$ in dx and dy are

$$dx = \frac{\partial x}{\partial \xi}d\xi + \frac{\partial x}{\partial \eta}d\eta \quad \text{and} \quad dy = \frac{\partial y}{\partial \xi}d\xi + \frac{\partial y}{\partial \eta}d\eta \tag{42}$$

They can be written in the form of a matrix, where the matrix of the partial derivatives is named Jacobian matrix of transformation.

$$\mathbf{J} = \begin{bmatrix} \frac{\partial x}{\partial \xi} & \frac{\partial x}{\partial \eta} \\ \frac{\partial y}{\partial \xi} & \frac{\partial y}{\partial \eta} \end{bmatrix} \tag{43}$$

$$\begin{bmatrix} dx \\ dy \end{bmatrix} = \mathbf{J}\begin{bmatrix} d\xi \\ d\eta \end{bmatrix} \tag{44}$$

The matrix to be invertible, the determinant need to be different from zero.

$$\text{det}\mathbf{J} = \frac{\partial x}{\partial \xi}\frac{\partial y}{\partial \eta} - \frac{\partial x}{\partial \eta}\frac{\partial y}{\partial \xi} \neq 0 \tag{45}$$

Considering the local basis functions of the finite elements to construct T_e transformation,

$$T_e : \begin{cases} x = \sum_{p=1}^{M} x_i\psi_i(\xi,\eta) \\ \\ y = \sum_{p=1}^{M} y_i\psi_i(\xi,\eta) \end{cases} \tag{46}$$

M represents the number of nodes in the element. Assuming a linear triangular element in the physical space, the local basis functions are linear in the master element and they are given by

$$\psi_0 = -\frac{1}{2}(\xi+\eta) \qquad \psi_1 = \frac{1}{2}(\xi+1) \qquad \psi_2 = \frac{1}{2}(\eta+1) \tag{47}$$

The final step is the transformation of the function $\mathbf{q}$ of x and y in the element Ω_e into $\mathbf{q}$ of ξ and η in the reference element $\hat{\Omega}$.

$$\mathbf{q}(x,y) = \mathbf{q}(x(\xi,\eta),y(\xi,\eta)) = \mathbf{q}(\xi,\eta) \tag{48}$$

where $x(\xi,\eta)$ and $y(\xi,\eta)$ are shown in the transformation T_e.

Following the integration requirement of the shallow water system, the transformation of volume integral to the local space is the equation 49

$$\int_{\Omega_e} \mathbf{q}(x,y)dxdy = \int_{\hat{\Omega}} \mathbf{q}(\xi,\eta)\ det\mathbf{J}(\xi,\eta)\ d\xi d\eta \tag{49}$$

having $det\mathbf{J}$ defined as the relation between the area in the physical element and the master element, as both spaces are analysed counterclockwise, if the determinant of the Jacobian is positive, the transformation is correct. The computation of the element boundary integrals, relate to the numerical flux, is given by

$$\int_{\Gamma_{ei}} \mathbf{H}_{ei}\phi d\Gamma = \int_{-1}^{1} \mathbf{H}_{ei}\phi\left(\xi(\theta),\eta(\theta)\right) det\mathbf{J}_{ei}d\theta \tag{50}$$

where

$$d\Gamma = det\mathbf{J}_{ei}\, d\theta = \sqrt{\left(\frac{\partial x}{\partial \theta}\right)^2 + \left(\frac{\partial y}{\partial \theta}\right)^2}\, d\theta, \quad (51)$$

θ represents a parameterization of the triangular element's edges, where it assumes values between -1 and 1, as shown in equations 52[1]:

$$e_{ei}^0 \left\{ \begin{array}{l} \xi^0 = -\theta \\ \eta^0 = \theta \end{array} \right. \qquad e_{ei}^1 \left\{ \begin{array}{l} \xi^1 = -1 \\ \eta^1 = -\theta \end{array} \right. \quad (52)$$

$$e_{ei}^2 \left\{ \begin{array}{l} \xi^2 = \theta \\ \eta^2 = -1 \end{array} \right. \quad (53)$$

As shown in figure 2, the parameter is applied in the master space, and it does not impact the physical space. Considering only the case of a triangle with straight

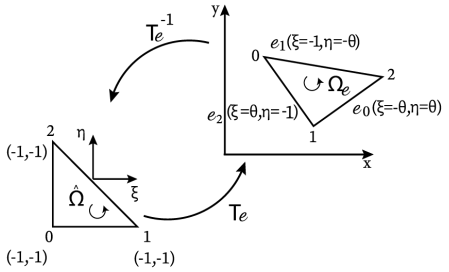

Figure 2: Transformation from element Ω_e to $\hat{\Omega}$ through T_e map

edges the Jacobian is a constant along the edge however, it depends on the number of the edge.

5.3. Legendre polynomials and system of equation

Following the Legendre polynomials for one-dimension, the two-dimension Legendre polynomial can be defined as a set of two-dimensional basis functions, defined in the interval [-1, 1]

$$\mathbf{q}(\xi, \eta, t) \;=\; \sum_{m=0}^{d+1} \phi_m(\xi, \eta)\, \mathbf{q}_m(t) \quad (54)$$

where $\mathbf{q}_m$ is the conservative vector, represented by

$$\mathbf{q}_m \;=\; (h_m \quad (hu)_m \quad (hv)_m) \quad (55)$$

and $(d+1)$ is the number of the basis functions based on the order k of the polynomial, it is given by

$$d + 1 \;=\; \frac{1}{2}(k+1)(k+2) \quad (56)$$

this equation follows Pascal's triangle. The system can be written as

$$\frac{\partial \mathbf{q}_n}{\partial t} \;=\; \hat{\mathbf{F}}_n \;-\; \hat{\mathbf{H}}_n^{int} \;-\; \hat{\mathbf{H}}_n^{bc} \;+\; \hat{\mathbf{S}}_n \;=\; \boldsymbol{\mathcal{R}}_n(q) \quad (57)$$

[1] In the notation ξ^p of the equation 52 p exemplifies the edge number, which coincides with the opposite node, this indexing is used for the normal vectors as well

where $\boldsymbol{\mathcal{R}}_n$ is defined as the residual and the other vectors are described by

$$\hat{\mathbf{F}}_n \;=\; \int_{-1}^{1} \int_{-1}^{-\xi} \mathbf{F}(\mathbf{q}) \cdot \nabla \phi_n d\xi d\eta \quad (58)$$

$$\hat{\mathbf{H}}_n^{int} \;=\; \sum_{\Gamma_e^{int}} \theta \int_{-1}^{1} \mathbf{H}(\mathbf{q}_{ei}; \mathbf{q}_{ie}; \mathbf{n}_{ei}) \phi_n d\theta \quad (59)$$

$$\hat{\mathbf{H}}_n^{bc} \;=\; \sum_{\Gamma_e^{bc}} \theta \int_{-1}^{1} \mathbf{H}(\mathbf{q}_{eb}; \mathbf{q}_b^{bc}; \mathbf{n}_{eb}) \phi_n d\theta \quad (60)$$

$$\hat{\mathbf{S}}_n \;=\; \int_{-1}^{1} \int_{-1}^{-\xi} \mathbf{s}\, \phi_n d\xi d\eta \quad (61)$$

it is important to notice that the Jacobians are constant since the triangle elements have straight edges, therefore they can be moved outside the integrals, $\theta = (\text{det}\mathbf{J})^{-1}\text{det}\mathbf{J}_{ei}$. [6]

6. Integrals discretization

The integration is computed on the master element by a two-dimensional Gaussian quadrature rule with g points (ξ, η) and weights w, the method applied in the flux gives

$$\hat{\mathbf{F}}_n \;=\; \sum_{b=1}^{g} w_b \left(\mathbf{F}_x(q(\xi_b, \eta_b)) \frac{\partial \phi_n(\xi_b, \eta_b)}{\partial x} + \mathbf{F}_y(q(\xi_b, \eta_b) \frac{\partial \phi_n(\xi_b, \eta_b)}{\partial y} \right) \quad (62)$$

where the partial derivation of ϕ_n is computed with the chain rule. The same procedure is practised on the source term,

$$\hat{s}_n \;=\; \sum_{b=1}^{g} w_b s(\xi_b, \eta_b) \phi_n(\xi_b, \eta_b) \quad (63)$$

The numerical flux regards only the edge, a one-dimensional element, therefore it is used the one-dimensional Gaussian quadrature rule with f points. In addition, θ-parametrisation is necessary to integrate along the edges. Applying the system in 52 onto the equations 59 and 60,

$$\hat{\mathbf{H}}_n^{int} \;=\; \sum_{\Gamma_e^{int}} \sum_{b=1}^{f} \theta w_b \mathbf{H}(\mathbf{q}_{ei}(\theta_b); \mathbf{q}_{ie}(-\theta_b); \mathbf{n}_{ei}) \phi_n(\theta_b) \quad (64)$$

$$\hat{\mathbf{H}}_n^{bc} \;=\; \sum_{\Gamma_e^{bc}} \sum_{b=1}^{f} \theta w_b \mathbf{H}(\mathbf{q}_{eb}(\theta_b); \mathbf{q}_b^{bc}(-\theta_b); \mathbf{n}_{eb}) \phi_n(\theta_b) \quad (65)$$

As q_{ei} and q_{ie} are related to the same edge, but considered in the two opposite directions, likewise $\pm\theta$ in q_{ei} have the opposite direction $\mp\theta$ in q_{ie}. [6]

The time integration follows the same procedure as 1D.

7. Results & discussion
7.1. One-dimensional cases

The one-dimensional code has three main variables to verify the accuracy of the solution: the degree of the polynomial, the number of Gauss points and the number of elements present in the mesh.

It has been considered the channel length of 20'000 metres and the seabed without friction. The initial conditions are a water depth of 20 m downstream and a flow rate of 4 m^3/s upstream. This case has been studied with a bump in the bathymetry. The bump was obtained through two different equations: a parabola and a sinusoidal equation

$$f(x) = \frac{a}{2}\left(cos\left(\frac{2\pi(x-x_0)}{L_b}\right)+1\right) \tag{66}$$

$$f(x) = a\left(1-\frac{4(x-x_0)^2}{L_b^2}\right) \tag{67}$$

where a is the amplitude or the height of the bump of 2 m, L_b is the length of the bump of 10'000 m and x_0 is the centre of the bump in the centre of the channel.

The two equations represent the difference in conjunction with the flat seabed. The parabola has a sharp angle while the sinusoidal function has a more regular joining. The results from the simulation with the parabola equation, for different even numbers of elements and Gauss-Legendre points, are shown in figures 3 to 5. The water surface results are accurately predicted even with a few elements and Gauss-Legendre points. While, the flow rate shows an oscillation, which reduces its intensity with the increase in the number of elements and Gauss-Legendre points.

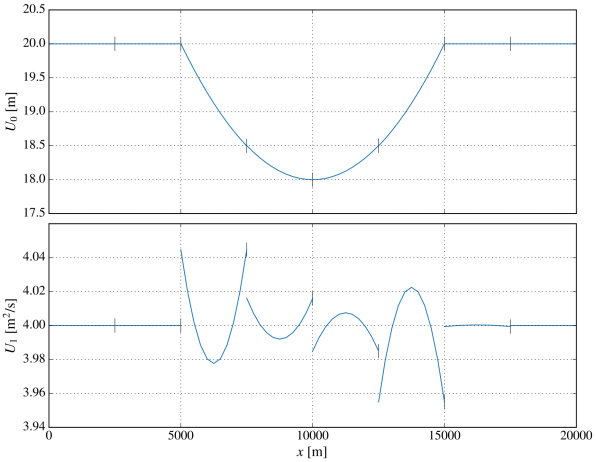

Figure 3: Solution with 8 elements, the second order of polynomial and 2 Gauss-Legendre points, with parabola bump function.

Figure 6 shows the discretization error as a function of the mesh size.

U_0, which represents the water depth, achieves a high level of accuracy in all cases. When U_1, which is the flow rate, a higher number of Gauss-Legendre points is needed to obtain the expected error decadence.

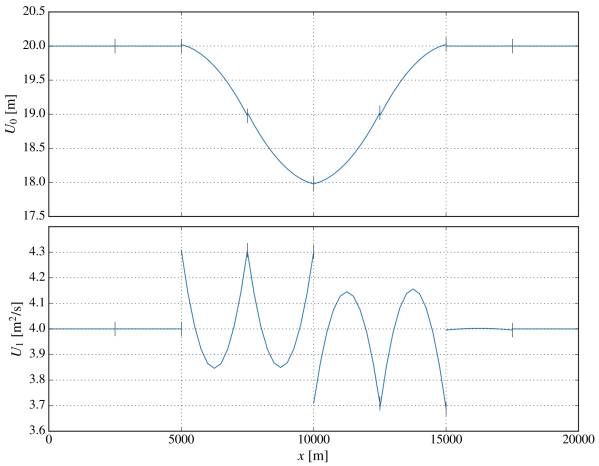

Figure 4: Solution with 8 elements, the second order of polynomial and 4 Gauss-Legendre points, with sinusoidal bump function.

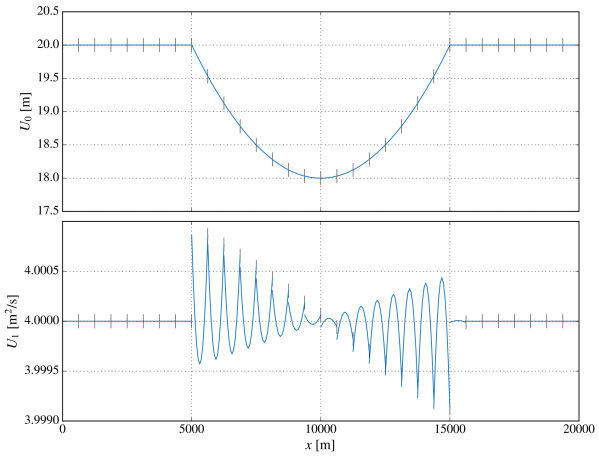

Figure 5: Solution with 32 elements, the second order of polynomial and 2 Gauss-Legendre points, with parabola bump function.

Considering the better results are errors for U_0. Therefore, the different numbers of Gauss-Legendre points were compared, and the best trend line is shown. It is important to point out that the minimum number of Gauss-Legendre points that can be exploited is equal to the degree of the polynomial g. Otherwise, there are not enough points to solve the polynomial.

The lowest error related to the number of elements is achieved with the number of points equal to $g+1$, however, this case never represents the finest error decay. The increase in the number of Gauss-Legendre points does not generate a consistent variation in the error after the $g+3$, as shown in figure 7. There is only a consistent improvement in the error associated with the increase in Gauss-Legendre points, from two to three or four points, which becomes negligible with the fourth degree of the polynomial, as shown in figure 8.

Comparing the three graphs 7 and 8, the increase of the polynomial degree minimises the error and the model requires a lower number of elements.

The solution has been studied with odd numbers of elements as well. Understanding of the effects of

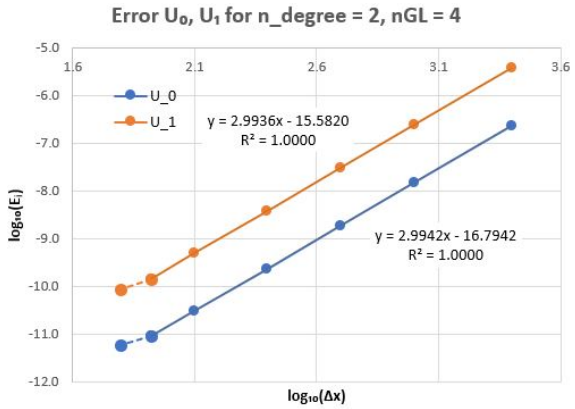

Figure 6: Error of U_0 and U_1 with even numbers of elements, the second order of polynomial 4 Gauss-Legendre points.

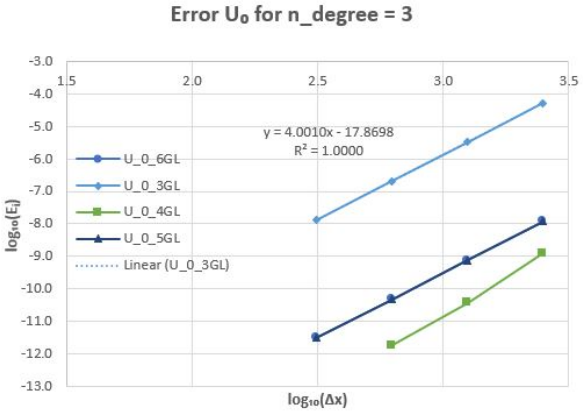

Figure 7: Comparison of the errors of U_0 of the third-order polynomial with different Gauss-Legendre points even number of elements and a parabola as bump function.

bathymetry when the variation from the flat seabed to the bump is within an element. The results show that the sinusoidal function gives a better degree of accuracy. As the function creates a more regular transition from the flat seabed to the bump, as it is possible to see in figure 4. Instead, the parabola function creates a sharp corner inside the element. All the previous considerations are valid for the error of the odd numbers of elements, even if the error trends do not show the decadence expected.

7.2. Two-dimensional cases

In the two-dimensional code has been considered the channel length of 20'000 m, the width of 4'000 m and the seabed is without friction. The mesh has a refinement of 250 m. It is shown in figure 10 with the boundary conditions.

The initial conditions are a water depth of 20 m downstream, named in figure 10 a BC100, a flow rate of 4 m^3/s upstream, called BC101 and a boundary condition at the wall of zero velocity, named BC102. These conditions describe a sub-critical flow.

It is important to notice that the Gauss-Legendre points are divided in internal and on the edges. The minimum number of Gauss-Legendre points inside the element in this case is 3, due to the second dimension. Moreover, there is a different correlation from the 1D model between the degree of the polynomial and the internal Gauss-Legendre points given by the quadrature rule.

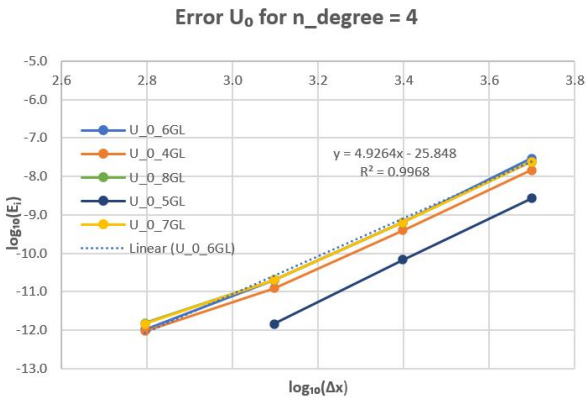

Figure 8: Comparison of the errors of U_0 of the fourth-order polynomial with different Gauss-Legendre points even number of elements and a parabola as bump function.

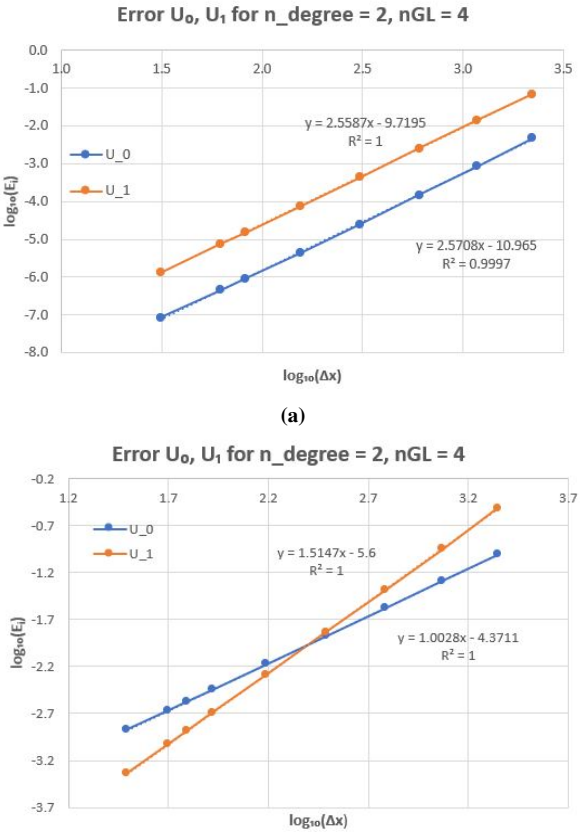

Figure 9: Error of U_0 and U_1 with odd numbers of elements: (a) the sinusoidal function for the bump and (b) the parabola function for the bump

The water surface results are accurately predicted in all cases run with different Gauss-Legendre points and degrees of polynomial. While the flow rate shows a decrease in accuracy with the increase of the polynomial, this unexpected result may be related to an error in the code. However, it was not found it.

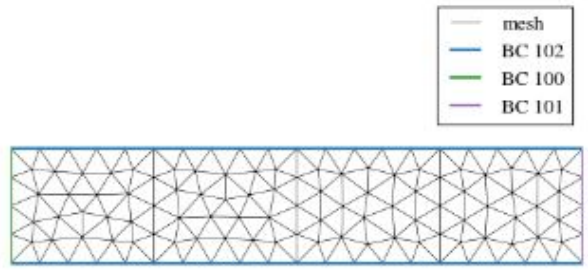

Figure 10: Mesh applied in the 2D code.

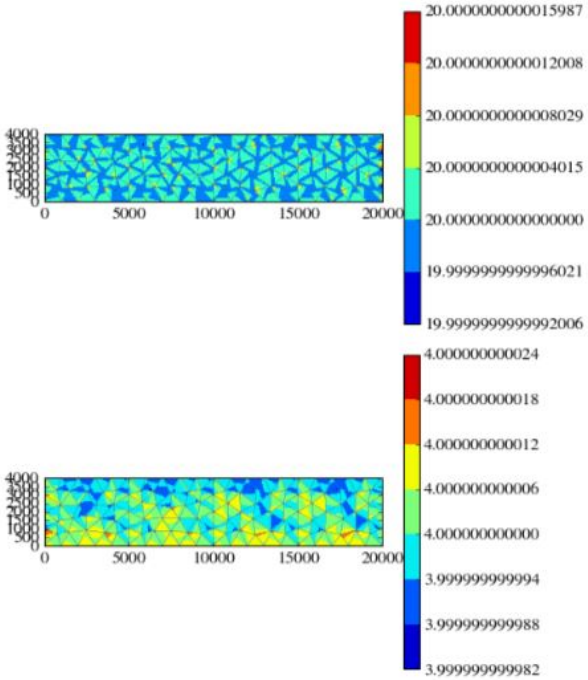

Figure 11: Solution with the fourth order of polynomial and 4 Gauss-Legendre points internal and on the edges.

8. Conclusions

The recent development of new turbine technologies opens new possibilities for the extraction of energy from tidal flow. Compared to other renewable energies, tidal power has considerable advantages. Its predictability enables the resource to be accurately quantified, unlike stochastic energy sources. It has a low environmental impact and no occupation of land.

This thesis studied the tidal resource assessment procedure for the situation of the current projects and developed a numerical method to analyse tidal hydrodynamics. The numerical method selected was the Discontinuous Galerkin method. Since it has the ability to use unstructured meshes and to model flows with significant horizontal velocities. In addition to the boundary condition directly implemented numerical flux, and provides higher accuracy within the flow field. This tool has a one-dimensional and two-dimensional versions.

The one-dimensional model developed presents the correct computation of the flow rate, the momentum flux in the local field and the water depth in all cases studied and presented. The precision of the model is confirmed by the error analysis, which is minimised by the refinement of the mesh and the increase of the polynomial order. This follows the theory, until the fifth order of the polynomial, where the round-off error starts to overcome the discretization error.

The two-dimensional model presents the correct computation of the flow rate, the momentum flux in the local field and the water depth in the case studied. However, the accuracy decrease and the residual increase with the increase in the polynomial degree, which suggests a problem in the code.

In summary, the numerical model has been proved useful for estimating the tidal stream's local velocities and water depth, in one-dimensional and two-dimensional. It can potentially be applied for tidal resource assessment and energy extraction analysis.

References

[1] S. Bhatia. 13 - tide, wave and ocean energy. In S. Bhatia, editor, *Advanced Renewable Energy Systems*, pages 307–333. Woodhead Publishing India, 2014.

[2] EMEC. Tidal devices, 2022.

[3] R. A. P. J. Marshall. *Atmosphere, Ocean and Climate Dynamics*. Academic Press, 2007.

[4] P. Novak, V. Guinot, A. Jeffrey, and D. Reeve. *Hydraulic Modelling - an Introduction*. 01 2010.

[5] D. Pugh. *Tides, Surges and Mean Sea-Level*. John Wiley and Sons, 1987.

[6] I. H. Shames. *Mechanics of Fluids*. McGraw-Hill, International Student Edition, 1982.